Technical Note

Dose and linear energy transfer distributions of primary and secondary particles in carbon ion radiation therapy: A Monte Carlo simulation study in water

Daniel Johnson, Yong Chen, Salahuddin Ahmad

Department of Radiation Oncology, Peggy and Charles Stephenson Cancer Center, The University of Oklahoma Health Sciences Center, Oklahoma 73104, USA

Received on: 31-03-2015 **Review completed on:** 02-07-2015 **Accepted on:** 07-07-2015

ABSTRACT

The factors influencing carbon ion therapy can be predicted from accurate knowledge about the production of secondary particles from the interaction of carbon ions in water/tissue-like materials, and subsequently the interaction of the secondary particles in the same materials. The secondary particles may have linear energy transfer (LET) values that potentially increase the relative biological effectiveness of the beam. Our primary objective in this study was to classify and quantify the secondary particles produced, their dose averaged LETs, and their dose contributions in the absorbing material. A 1 mm diameter carbon ion pencil beam with energies per nucleon of 155, 262, and 369 MeV was used in a geometry and tracking 4 Monte Carlo simulation to interact in a 27 L water phantom containing 3000 rectangular detector voxels. The dose-averaged LET and the dose contributions of primary and secondary particles were calculated from the simulation. The results of the simulations show that the secondary particles that contributed a major dose component had LETs <100 keV/μm. The secondary particles with LETs >600 keV/μm contributed only <0.3% of the dose.

Key words: Carbon ion therapy, dose, linear energy transfer distributions

Introduction

Ion beam radiotherapy has the potential to achieve dose conformity indices higher than those of traditional photon therapy. Carbon ion therapy may be one of the most promising forms of light-ion therapy, and studies regarding the production of secondary particles from the interaction of carbon ions in water-like absorber materials, and subsequently the interactions of secondary particles in the same materials, predict the importance of this therapy for clinical use. Coupled with a greater relative biological effectiveness (RBE), the potentially higher therapeutic ratio implies an increase in the tumor control probability, and a reduction of the normal tissue complication probability.[1-4]

Dose conformity in ion beam therapy is enhanced through the properties of the Bragg peak. Increased linear energy transfer (LET) along the beam path implies a greater ionization density, and thus an enhanced RBE. It is generally accepted that the RBE is dependent upon the dose, dose fractionation, tissue type, biological endpoint, and the local particle energy spectrum, which is usually referred as radiation quality and can be characterized by the LET. LET definitions are based on the stopping power values used to describe the gradual loss of energy of the incoming ion per unit path length as it penetrates an absorbing material; it is the sum of the electronic and nuclear collision stopping power and the radioactive

Address for correspondence:
Prof. Salahuddin Ahmad,
Department of Radiation Oncology, Peggy and Charles Stephenson Cancer Center, The University of Oklahoma Health Sciences Center, 800 N.E. 10th Street, OKCC L100, Oklahoma City, OK, 73104, USA.
E-mail: salahuddin-ahmad@ouhsc.edu

Access this article online	
Quick Response Code:	Website: www.jmp.org.in
	DOI: 10.4103/0971-6203.170785

How to cite this article: Johnson D, Chen Y, Ahmad S. Dose and linear energy transfer distributions of primary and secondary particles in carbon ion radiation therapy: A Monte Carlo simulation study in water. J Med Phys 2015;40:214-9.

stopping power. The contributions of nuclear interactions are crucial for light-ion beam therapy, as the production of secondary particles having significant LET values can cause a potential increase in the RBE of the beam.

For a secondary particle with specific charge and velocity, the term LET is determined by the energy transferred from a large number of particles of the same type to a localized region, on average, per unit path length. The dose-averaged LET used in this study is defined as

$$\overline{L_d(d)} = \frac{\int_0^\infty \phi_E(d) S^2(E) dE}{\int_0^\infty \phi_E(d) S(E) dE} \quad (1)$$

where ϕ_E is the particle fluence in energy E, at the depth d, and S (E) is the stopping power of a specific particle type of energy E.

Accelerators may produce a variety of ion beams, of which proton and carbon ion beams are the most common in clinical use. With the comparable dose conformity of protons and carbon ions, they differ most in their RBE, because of their different LET.[5] Due to a greater distribution of dose beyond the Bragg peak, carbon beams are not generally considered to be dosimetrically superior to protons; the correlations between LET, RBE, and an ion's charge and mass are not as yet well-established.[6]

Brahme determined values, based on biological parameters, that place an optimum LET for cell killing at 25–75 keV/μm, while urging minimization of the LET to normal tissues.[6] Studying a number of potential light-ion beams, Kempe *et al.* concluded the optimum hadronic therapy to be that with lithium pencil beams (followed by beryllium and boron), possessing a localized high-LET (>20 keV/μm) component at the end of its range while maintaining low (<10 keV/μm) LET values in normal tissues.[7] In view of the beam path of the carbon beam is littered with a variety of secondary particles possessing a wide range of LET values, more reliable model parameters and clinical trials are needed for exploration of the advantage of carbon ion radiation therapy.[8,9]

With the increasing popularity of clinical heavy particle radiotherapy, proton LET simulations are of increasing relevancy.[10] The logical progression in the technology of particle therapy may be the eventual adoption of clinical carbon ion beams. Classifying as well as quantifying the secondary particles produced, their dose averaged LETs, and their dose contributions in the absorbing material are the primary focus of the current carbon ion beam simulation.

Materials and Methods

A simulation program was constructed with the Monte Carlo code geometry and tracking 4 (GEANT4) provided by Conseil Européen pour la Recherche Nucléaire. GEANT4 is an open-source code that offers an abundant set of physics processes incorporating various particle interactions that occur during beam transport. As an object-oriented toolkit, GEANT4 (version 9.2) provides high flexibility to users constructing user-defined lists of physics processes. Within the GEANT4 environment, pristine Bragg peaks resulting from carbon ion interactions were simulated in this study with use of processes arising out of electromagnetic interactions (EMIs) and hadronic interactions (HIs). The EMI governs a particle's energy loss and straggling with atomic electrons and multiple scattering with atomic nuclei. The HI defines an ion's elastic and inelastic scattering and nuclear interactions with atomic nuclei in the medium.

The code offers wide flexibility for choosing different physics models for each interaction process. The EMI energy loss processes of hadrons were modeled through the low energy physics implementation to improve the Bragg peak position accuracy. The HIs of protons and neutrons were simulated through the low-energy elastic interactions, whereas a binary cascade model simulated inelastic scattering processes. The choice for the physics list came from previous experience at our institution.[11-14]

A quantum molecular dynamics model simulated additional inelastic light-ion interactions. These processes have been established in the medical physics community[15,16] in order to optimize calculations from simulations that agree well with available experimental data. Standard EMIs were used for gamma rays, electrons, and positrons. The range cut used in the simulation was 0.1 mm for gammas, electrons, and positrons in the water phantom which represents the energy cutout of 1.1134 keV for gamma, 85.1138 keV for electron, and 83.8172 keV for positron.

A Gaussian pencil beam with a full-width-half-maximum value of 1 mm composed of 1 million incident carbon ions was used in all simulations. A 1% uncertainty of the simulation is assigned to the primary particle count only in each detector voxel. Repeated simulations, each having a unique random-number seeding, were utilized to determine the total number of incident particles required to yield a maximum standard deviation that is <1% for all detector voxels, while simultaneously optimizing the duration of the calculation. The incident energies per nucleon of the carbon ion beams were 155, 262, and 369 MeV/u. The energies used also had a Gaussian distribution of 1% full-width-half-maximum. A 27 L cubic water phantom (30 cm × 30 cm × 30 cm) was used as a target to mimic a human body, which consisted of 3000 packed rectangular detector voxels (30 cm × 30 cm × 0.1 mm). The beam was situated to strike the broad face of the detector voxels at 90° to a centralized position. A schematic drawing is shown in Figure 1. The simulated energy depositions within each detector voxel were used for determination of

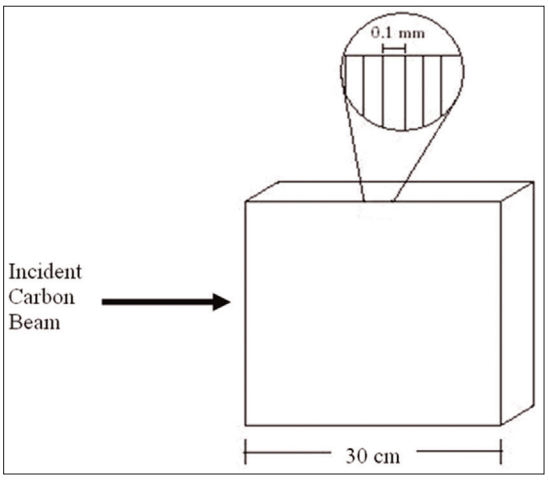

Figure 1: Simulated water phantom is a cube of 30 cm per side. The cube is comprised of 0.1 mm detector "voxels" oriented perpendicular to the incident carbon ion beam

the pristine Bragg peaks for the three carbon ion beams of different energies. The dose averaged LET for a specific particle in the detector at depth d was calculated by the following equation in order to be used in the Monte Carlo simulation:

$$\overline{L_d(d)}^{MC} = \frac{\int dE(d) \times (dE(d)/dX)}{\int dE(d)} \quad (2)$$

where dE is the energy deposit and the dE/dX is the corresponding stopping power.

The energy deposition, total kinetic energy, fluence, and dose-averaged LETs of each produced secondary particle within each detector voxel were determined for the study of their variations with depth. The secondary particles investigated in this study were gamma rays, neutrons, electrons, positrons, protons, deuterons, tritons, alpha particles, ^{3}He, ^{6}Li, ^{7}Li, ^{7}Be, ^{9}Be, ^{10}Be, ^{10}B, ^{11}B, ^{11}C, ^{12}C, ^{13}C, ^{14}C, ^{13}N, ^{14}N, ^{15}N, and ^{16}O. One-dimensional distributions of the dose-averaged LET were calculated for all primary and secondary particles resulting from the simulations.

Results and Discussion

Region "A" covers the beam path from the phantom surface at the beam entrance up to the 90% distal edge of the Bragg peak and region "B" covers the beam path from the 90% distal edge of the Bragg peak up to 5 cm past the Bragg peak. The percentage of the total dose deposited in regions "A" and "B" of the phantom contributed by the primary and the secondary particles is shown in Tables 1 and 2, respectively, for three beam energies. The percentage dose contribution from the primary beam (^{12}C) in regions "A" and "B" dropped as the incident energy increased: about 93.54%, 85.61%, and 76.60% in region "A" [Table 1] and 28.97%, 17.77%, and 13.08% in region "B" [Table 2], with carbon ion beam energies per nucleon of 155, 262, and 369 MeV, respectively. The top four identified secondary particle dose contributors were protons, ^{11}C, alpha particles, and ^{11}B [Table 1]. These four secondary particles contributed together 4.17%, 9.26%, and 15.21% of the integrated dose in region "A" and 49.10%, 55.13%, and 58.07% of the integrated dose in region "B" for carbon ion beam energies per nucleon of 155, 262, and 369 MeV, respectively.

Table 1: Percentage of the total dose deposited in a region of the phantom that extends from the phantom surface at the beam entrance up to the 90% distal edge of the Bragg peak, contributed by the primary and the secondary particles for three beam energies

Particle	*Incident carbon ion energy per nucleon*		
	155 MeV/u	*262 MeV/u*	*369 MeV/u*
^{12}C	93.54	85.61	76.60
Proton	1.36	3.75	6.90
^{11}C	1.12	2.27	3.34
Alpha	1.08	2.12	3.42
^{11}B	0.75	1.52	2.28
^{10}B	0.61	1.12	1.55
^{7}Be	0.32	0.58	0.82
Deuteron	0.30	0.61	0.88
^{3}He	0.22	0.41	0.60
^{6}Li	0.17	0.33	0.50
Electron	0.02	0.76	1.78
All others*	0.52	0.92	1.33

*Total contributions from ^{16}O, ^{13}N, ^{14}N, ^{15}N, ^{13}C, ^{14}C, ^{7}Li, ^{9}Be, ^{10}Be, triton, positron, gamma

Table 2: Percentage of the total dose deposited in a region of the phantom that extends from the 90% distal edge of the Bragg peak up to 5 cm past the Bragg peak, contributed by the primary and the secondary particles for three beam energies

Particle	*Incident carbon ion energy per nucleon*		
	155 MeV/u	*262 MeV/u*	*369 MeV/u*
^{12}C	28.97	17.77	13.08
Alpha	27.65	25.16	23.93
Proton	14.97	18.92	21.73
^{11}B	6.47	10.98	12.37
Deuteron	4.36	4.12	3.90
^{7}Li	3.35	3.13	2.60
^{6}Li	2.93	3.37	3.06
^{3}He	2.60	3.48	3.68
^{10}B	2.30	4.62	6.53
^{9}Be	1.60	2.28	2.07
Triton	1.54	1.20	1.09
^{7}Be	1.50	2.92	3.84
^{10}Be	1.41	1.59	1.34
Electron	0.17	0.23	0.51
All others*	0.18	0.23	0.25

*Total contributions from ^{16}O, ^{13}N, ^{14}N, ^{15}N, ^{11}C, ^{13}C, ^{14}C, positron, gamma

The relative dose contribution of the primary and the above four secondary particles as a function of phantom depth (from 5 cm prior to up to 5 cm distal to the Bragg peak) for carbon ion beam energies per nucleon of 155, 262, and 369 MeV is shown in Figures 2a, 3a, and 4a, respectively. These figures clearly show large dose contributions from protons, alpha particles, and ^{11}B in the tail area (Bragg peak to 5 cm distal to the Bragg peak) with an indication of continuing large dose contributions beyond that depth.

The dose-averaged LET of the primary and the secondary particles in regions "A" and "B" for the three beam energies are shown in Tables 3 and 4, respectively. The average LET for region "A" was <10 keV/μm for the positrons, electrons, gammas, tritons, deuterons, and protons; and between 10 and 100 keV/μm for the primary particle (^{12}C) and the secondary particles ^{3}He, ^{6}Li, ^{7}Li, ^{7}Be, ^{9}Be, ^{10}Be, ^{10}B, ^{11}B, ^{11}C, and alpha; and between 600 and 1000 keV/μm for the secondary particles of ^{13}C, ^{14}C, ^{13}N, ^{14}N, ^{15}N, and ^{16}O, independent of the carbon ion energy per nucleon.

The secondary particles in region "A" with a dose-averaged LET <10 keV/μm were also found to have the same dose-averaged LET in region "B". The dose-averaged LET lay between 10 keV/μm and 100 keV/μm for alphas, ^{3}He, ^{6}Li, ^{7}Li, ^{9}Be, and ^{10}Be, and between 600 and 1000 keV/μm for primary (^{12}C), and secondary particles of ^{11}C, ^{13}C ^{14}C, ^{13}N, ^{14}N, ^{15}N, and ^{16}O, irrespective of carbon ion energy per nucleon for region "B." The dose-averaged LET of the primary (^{12}C), as well as the four secondary particles of protons, ^{11}C, alphas, and ^{11}B as a function of phantom depth (from 5 cm prior to up to 5 cm distal to the Bragg peak) for carbon ion beam energies per nucleon of 155, 262, and 369 MeV are shown in Figures 2b, 3b, and 4b, respectively. The integrated dose contributions from all secondary particles that had higher average LET

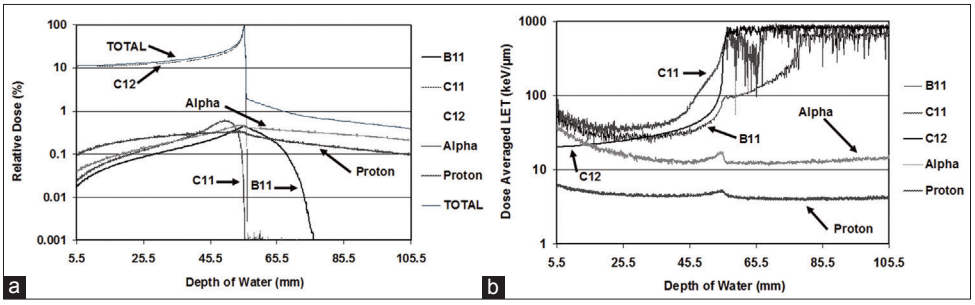

Figure 2: Plots of relative dose (a) and dose-averaged linear energy transfer (b) as they vary with depth for the primary 155 MeV/u carbon ion beam and most prominent secondary beam products. Displayed is a range of the phantom that includes 5 cm of depth preceding and succeeding the Bragg peak

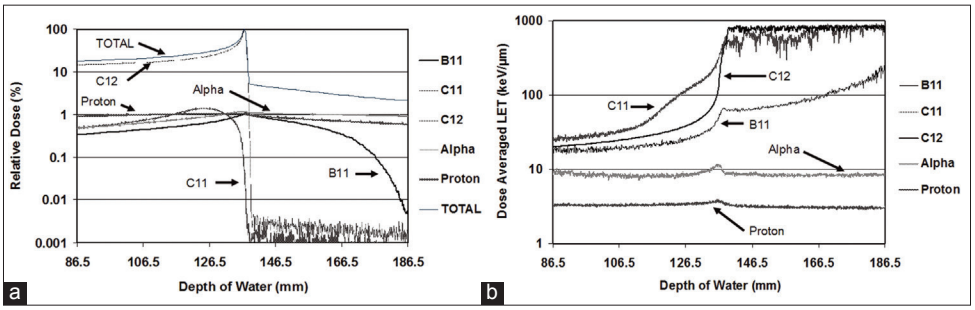

Figure 3: Plots of relative dose (a) and dose averaged linear energy transfer (b) as they vary with depth for the primary 262 MeV/u carbon ion beam and most prominent secondary beam products. Displayed is a range of the phantom that includes 5 cm of depth preceding and following the Bragg peak

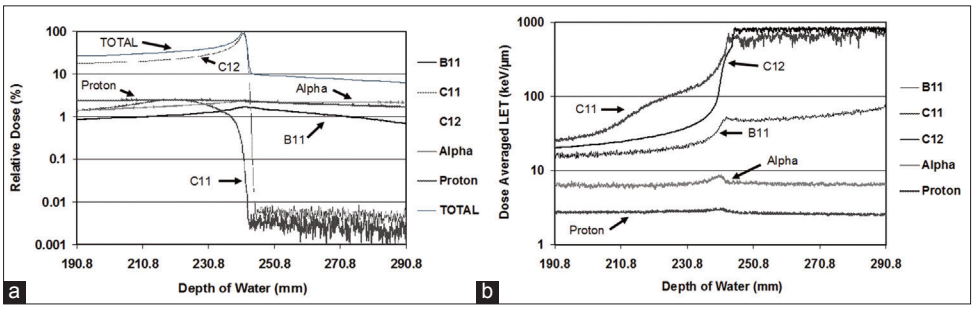

Figure 4: Plots of relative dose (a) and dose-averaged linear energy transfer (b) as they vary with depth for the primary 369 MeV/u carbon ion beam and most prominent secondary beam products. Displayed is a range of the phantom that includes 5 cm of depth preceding and following the Bragg peak

Table 3: Average LET (keV/μm) in a region of the phantom that extends from the phantom surface at the beam entrance up to the 90% distal edge of the Bragg peak, contributed by the primary and secondary particles for three beam energies

Particle	*Incident carbon ion energy per nucleon*		
	155 MeV/u	*262 MeV/u*	*369 MeV/u*
Positron	0.27	0.28	0.28
Electron	0.36	0.48	0.47
Gamma	1.70	1.73	0.51
Proton	5.08	3.80	3.19
Deuteron	6.76	5.32	4.67
Triton	8.67	7.49	6.70
^{3}He	20.38	15.10	12.42
Alpha	21.10	15.76	13.17
^{6}Li	30.26	20.06	16.16
^{7}Li	33.34	21.51	17.24
^{12}C	33.59	23.19	18.60
^{11}B	43.53	26.07	19.48
^{7}Be	43.63	27.69	21.85
^{9}Be	44.37	29.06	22.84
^{10}B	51.38	32.95	25.64
^{10}Be	58.45	36.03	28.81
^{11}C	74.86	48.08	37.03
^{13}C	685.3	769.9	800.3
^{14}C	723.6	787.1	815.4
^{13}N	865.2	949.9	983.3
^{14}N	906.1	969.0	994.9
^{15}N	934.1	979.9	989.9
^{16}O	1004.0	958.3	941.8

LET: Linear energy transfer

Table 4: Average LET (keV/μm) in a region of the phantom that extends from the 90% distal edge of the Bragg peak up to 5 cm past the Bragg peak, contributed by the primary and secondary particles for three beam energies

Particle	*Incident carbon ion energy per nucleon*		
	155 MeV/u	*262 MeV/u*	*369 MeV/u*
Positron	0.28	0.28	0.29
Electron	0.36	0.42	0.46
Gamma	1.17	1.16	1.04
Triton	3.69	2.83	2.45
Deuteron	3.75	2.83	2.39
Proton	4.11	3.10	2.62
Alpha	12.94	8.414	6.584
^{3}He	15.17	9.646	7.163
^{7}Li	30.26	18.06	14.17
^{6}Li	34.06	19.84	14.86
^{10}Be	70.53	34.56	26.54
^{9}Be	84.67	38.60	28.21
^{7}Be	169.4	57.79	41.20
^{11}B	416.0	103.0	54.84
^{10}B	456.9	184.7	80.61
^{11}C	716.0	666.8	652.4
^{14}C	756.0	800.2	814.6
^{13}C	802.3	796.5	806.1
^{12}C	804.5	789.4	780.0
^{16}O	852.2	903.5	924.9
^{13}N	932.0	974.6	989.2
^{15}N	952.2	952.1	960.0
^{14}N	970.4	981.0	984.4

Contd...

Table 4: Continued...

LET: Linear energy transfer

values (>600 keV/μm) were <0.1% and <0.3%, in regions "A" and "B," respectively, for all three beam energies. The dose contributions from secondary particles predominantly occurred when dose-average LETs were <100 keV/μm.

The simulation thus revealed that those secondary particles that contributed considerable dose components had dose-averaged LETs most commonly of <100 keV/μm. The secondary particles in region "A" that possess dose-averaged LET values within the range of 10–100 keV/μm, known to be of the greatest biological significance, contributed little relative dose. The primary particle beam dominated the relative dose contribution in this region, and maintained an optimal dose-averaged LET between 19 and 34 keV/μm. In region "B," it is seen that the dose from the primary particles dropped substantially, whereas its dose-averaged LET increased by more than 20-fold. The secondary particles possessing both an adequate dose deposition (>10%) and a dose-averaged LET within the ideal range were found to be ^{11}B and alpha.

Conclusions

The present simulation revealed that those secondary particles that contributed major dose components in carbon ion therapy were those whose LETs were most commonly <100 keV/μm. The dose contributions from secondary particles that had higher averaged LET values of >600 keV/μm are almost negligible (<0.3%), independent of the dose regions and beam energies used in this study.

Acknowledgment

A part of this work has been presented at the 54th American Association of Physicists in Medicine Annual meeting in Charlotte, NC, 2012.

Financial support and sponsorship

Nil

Conflicts of interest

There are no conflicts of interest.

References

1. Kraft G, Arndt U, Becher W, Schardt D, Stelzer H, Weber U, *et al*. Heavy ion therapy at GSI. Nucl Instrum Methods Phys Res A 1995;367:66-70.
2. Amaldi U, Kraft G. Radiotherapy with beams of carbon ions. Rep Prog Phys 2005;68:1861-82.
3. Schulz-Ertner D, Jäkel O, Schlegel W. Radiation therapy with charged particles. Semin Radiat Oncol 2006;16:249-59.
4. Schulz-Ertner D, Tsujii H. Particle radiation therapy using proton and heavier ion beams. J Clin Oncol 2007;25:953-64.
5. Curtis SB. Calculated LET distributions of heavy ion beams. Int J Radiat Oncol Biol Phys 1977;3:87-91.
6. Brahme A. Recent advances in light ion radiation therapy. Int J Radiat Oncol Biol Phys 2004;58:603-16.
7. Kempe J, Gudowska I, Brahme A. Depth absorbed dose and LET distributions of therapeutic 1H, 4He, 7Li, and 12C beams. Med Phys 2007;34:183-92.
8. Sørensen BS, Overgaard J, Bassler N. *In vitro* RBE-LET dependence for multiple particle types. Acta Oncol 2011;50:757-62.
9. Wilkens JJ, Oelfke U. Direct comparison of biologically optimized spread-out bragg peaks for protons and carbon ions. Int J Radiat Oncol Biol Phys 2008;70:262-6.
10. Grassberger C, Paganetti H. Elevated LET components in clinical proton beams. Phys Med Biol 2011;56:6677-91.
11. Chen Y. Nuclear Interactions and Relative Biological Effectiveness in Proton Radiation Therapy: A Simulation Study with GEANT4. Ph.D. Dissertation. University of Oklahoma Health Sciences Center, Oklahoma City, Oklahoma, USA; 2010.
12. Chen Y, Ahmad S. Empirical model estimation of relative biological effectiveness for proton beam therapy. Radiat Prot Dosimetry 2012;149:116-23.
13. Chen Y, Ahmad S. Evaluation of inelastic hadronic processes for 250 MeV proton interactions in tissue and iron using GEANT4. Radiat Prot Dosimetry 2009;136:11-6.
14. Lau A, Chen Y, Ahmad S. Yields of positron and positron emitting nuclei for proton and carbon ion radiation therapy: A simulation study with GEANT4. J Xray Sci Technol 2012;20:317-29.
15. Böhlen TT, Cerutti F, Dosanjh M, Ferrari A, Gudowska I, Mairani A, *et al*. Benchmarking nuclear models of FLUKA and GEANT4 for carbon ion therapy. Phys Med Biol 2010;55:5833-47.
16. Lechner A, Ivanchenko VN, Knobloch J. Validation of recent Geant4 physics models for application in carbon ion therapy. Nucl Instrum Methods Phys Res Sect B 2010;268:2343-54.